lubricants

MDPI

Article

Employment of Micro- and Nano-WS_2 Structures to Enhance the Tribological Properties of Copper Matrix Composites

Marco Freschi [1,*], Matteo Di Virgilio [1,*], Gabriele Zanardi [1], Marco Mariani [2], Nora Lecis [2] and Giovanni Dotelli [1]

[1] Department of Chemistry, Materials and Chemical Engineering "Giulio Natta", Politecnico di Milano, 20133 Milano, Italy; gabriele1.zanardi@mail.polimi.it (G.Z.); giovanni.dotelli@polimi.it (G.D.)
[2] Department of Mechanical Engineering, Politecnico di Milano, 20156 Milano, Italy; marco.mariani@polimi.it (M.M.); nora.lecis@polimi.it (N.L.)
* Correspondence: marco.freschi@polimi.it (M.F.); matteo.divirgilio@polimi.it (M.D.V.); Tel.: +39-0223993232 (M.F. & M.D.V.)

Abstract: Friction and wear are responsible for around 23% of the energy consumption in transportation, manufacturing, power generation, and residential sectors. Employed components are exposed to a wide range of operational conditions, therefore a suitable material design is fundamental to decreasing tribological issues, energy consumption, costs, and environmental impact. This study aims to analyze the effect of different solid lubricants on the suitability of copper matrix composites (CuMCs) as a potential solution to reduce the depletion of sliding electrical contacts working under extreme conditions. CuMCs samples are produced by cold-pressing and sintering to merge a high electrical conductivity with the lubricant effect supplied by different species, namely tungsten disulfide micro-powder (WS_2), inorganic fullerene-like (IF) tungsten disulfide nanoparticles, and graphene nanoplatelets (GNP). The crystalline structure of the pristine and composite materials is characterized via XRD. The electrical tests show a small decrease of conductivity compared to pure copper, due to the insulating effect of WS_2; however, the measured values are still adequate for conduction purposes. Micro-scratch and wear tests highlight the positive effect of the combination of WS_2 structures and GNP. The friction coefficient reduction leads to the possibility of extending the lifetime of the components.

Keywords: solid lubricants; friction; wear; inorganic fullerenes; nanoparticles; composite material

Citation: Freschi, M.; Di Virgilio, M.; Zanardi, G.; Mariani, M.; Lecis, N.; Dotelli, G. Employment of Micro- and Nano-WS_2 Structures to Enhance the Tribological Properties of Copper Matrix Composites. *Lubricants* **2021**, *9*, 53. https://doi.org/10.3390/lubricants9050053

Received: 2 February 2021
Accepted: 5 May 2021
Published: 7 May 2021

1. Introduction

Adequate lubrication is fundamental to improve the tribological properties and the long-term reliability of sliding electrical contacts [1–3], that are critical components in a wide range of devices such as direct current (DC) electromotors, alternators, house appliances, and slip rings [2,4–7]. Solid lubricants are drawing much attention and currently occupy a considerable portion of the research effort in this field, mostly for those applications in which the operating conditions are extreme and forbid the employment of liquid lubricants [8,9]. These species exhibit a layered molecular structure, characterized by weakly bonded planes of closely packed atoms, which allows a favorable orientation to attenuate the shear strength. Therefore, they promote an easier sliding and directly contribute to the minimization of friction and wear via the formation of a thin tribo-film between the mating materials in the specific operating environment [5].

Transition metal dichalcogenides (TMDs) such as molybdenum disulfide (MoS_2) and tungsten disulfide (WS_2), graphite, and graphene nanoplatelets (GNP) are the leading exponents of these lamellar solids. The combination of one or more of these materials with a compatible metal matrix allows to attain a two-phase or multi-phase self-lubricating metal matrix composite (MMC), in which the chemical and physical individuality of the phases is preserved while appropriately blending their properties [10]. Copper matrix composites

(CuMCs) are considered to be adequate for low-voltage and low-current applications due to stable low contact resistance, minimum heating, and a reduced wear rate [11].

WS_2 could represent an appropriate candidate for the manufacturing of particle-reinforced copper-based materials with enhanced tribological features [12]. This TMD strongly resembles to graphite, as it possesses a stratified crystal framework. Its peculiar properties are related to an anisotropic structure consisting of a central sheet of tungsten atoms covalently bonded with upper and lower layers of sulfur atoms, molding either a hexagonal or a rhombohedral polymorph [13,14]. The sandwiches are instead weakly bound by means of van der Waals forces, guaranteeing an intrinsic tribo-activity through the generation of a tribo-film that reduces friction coefficient and wear rate. Nonetheless, its expensiveness is a deterrent for being sufficiently competitive with MoS_2, despite it displays other fascinating features such as high chemical inertness, lower humidity sensitivity, and powder dispersibility [12,13,15].

Inorganic fullerene-like (IF) tungsten disulfide nanoparticles are closed nanoarchitectures of tungsten disulfide, firstly observed in 1992 by Tenne et al. [16]. The great advantage of these cage-like nanoparticles is their capability of outperforming other solid lubricants under harsh conditions since the closed structure forces the exposition of van der Waals surfaces without dangling bonds to the tribological interface [17]. They can contribute to lubrication on three different levels, allowing a long-term wear resistance, as studied by Rapoport et al. [18,19], Tevet et al. [20], and Uflyand et al. [21]. Firstly, due to rolling between mating surfaces, promoted by their spherical shape and high mechanical stability, IF nanoparticles act as ball bearings, reducing the friction coefficient especially at low loading levels. Then, sliding of IF nanoparticles lowers metal-to-metal contact through a physical separation, providing low friction and easy shearing thanks to their low surface energy and robustness. Finally, the special feature of IF nanoparticles is appreciated mostly at high loading levels through exfoliation, which consists of a gradual transfer of WS_2 layers. The exfoliated layers deposit on the asperities of the mating surfaces providing easy shearing, an enhanced lubrication and a prolonged serviceability [18–21]. Moreover, this process reduces local heating and hence plastic deformation of the underlying metal surface, further lessening wear issues. Despite extensive exfoliation eventually degrades the IF nanoparticles, they are able to behave as a reservoir of solid lubricant after high levels of wear, inasmuch as the released WS_2 sheets can be oxidized to form a tungsten oxide film, which is a good lubricant itself [22]. Chemical inertness, high temperature and oxidation resistances, robustness, and exceptional mechanical properties complete their array of properties [23,24] and make them trustworthy candidates to produce self-lubricating metal matrix composites. Amongst the several preparation methods, the bulk synthesis realized by Feldman et al. [25,26] is drawing particular attention. It is based on the reaction of solid tungsten trioxide (WO_3) powder in H_2S/H_2-rich atmosphere at about 850–900 °C. The growth mechanism of the nanoparticle starts from the surface of the oxide, which reacts with H_2S to form one or two closed monomolecular layers of WS_2 in the first few seconds. Then, H_2 diffusion reduces the inner oxide to a $W_{18}O_{49}$ intermediate. Finally, the core is progressively converted layer by layer into the hollow IF structure through a slow diffusion-controlled reaction, which lasts for 30–120 min. Since the incipient oxide particle serves as a template, its size directly determines the final size of the IF nanoparticle. This quasi-epitaxial growth mode gives rise to an almost perfect crystalline structure.

GNP are nanoflakes composed of few layers of platelet-shaped graphene sheets with variable thickness (0.7–100 nm), lateral size, and carbon-to-oxygen atomic ratio. Large scale-production of this material typically relies upon liquid phase exfoliation, but ball milling, microwave radiation on acid-intercalated graphite and shear-exfoliation are other widespread techniques. Good mechanical toughness, high hardness, superior tribological behavior, excellent thermal and electrical conductivities, light weight, high aspect ratio, and low cost make them ideal for several fields of application, such as the production of CuMCs working under humid environments [27–30]. Preparation of Cu-GNP composites requires that the carbonaceous reinforcement maintains its structural integrity

while being homogeneously incorporated and dispersed into the metal matrix. One of the most widespread techniques to fulfil these tasks is powder metallurgy (PM), which includes a ball milling step aimed at discouraging the natural agglomeration tendency of graphene, fostered by its large surface area [31,32]. However, mechanical milling should be carefully conducted since it could force structural damages and increase the density of defects on graphene platelets. Besides, high temperatures during powders' compacting and sintering steps might cause the formation of metallic carbides, which are detrimental for the final mechanical characteristics of the composite [33].

Strong scientific investigation is being performed to enhance the tribological performances of metals and alloys. Laser nanostructuring could be considered a fascinating technique, as proposed by Bonse et al. [34]. They have generated homogeneous laser-induced periodic surface structures (LIPSS) on 100Cr6 steel and titanium alloy (Ti6Al4V) through irradiation with multiple femtoseconds laser pulses. Reciprocal sliding in two different media—i.e., paraffin oil and commercial engine oil (Castrol VP-1)—has enabled elucidation of the tribological performances of the treated materials. Laser-processed 100Cr6 steel demonstrated a very low friction coefficient (0.15) in both lubricants. Differently, nanostructured Ti6Al4V displayed high and fluctuating friction coefficient values (from 0.2 to 0.6) in paraffin oil, while engine oil favored a reduction up to 0.12–0.14. This result has been explained by an advantageous combination of LIPSS and additives contained in engine oil, which efficiently cover the nanostructured surface. To verify the benefits of surface texturing on tribological properties, Gnilitskyi et al. [35] have imprinted highly uniform LIPSS on X5CrNi1810 stainless steel discs, exploiting optical femtosecond pulses. Tribological tests, conducted in a chamber filled with 20 mL of commercial motor oil (Shell Elix Synthetic 5w-40), have highlighted a sensible decrease of friction coefficient and wear from an unpatterned reference sample (about 0.2 and 6×10^{-2} mm^3, respectively) to the patterned one (about 0.15 and 3.5×10^{-2} mm^3, respectively). The produced surface grooves played a fundamental role as lubricant reservoir during the counterparts' contact and as debris pockets to minimize the abrasion caused by particles spread on the interface. Nonetheless, the employment of appropriate lubricating agents appears to be indispensable in attaining more convincing frictional features.

Authors are testing different solutions and preparation procedures to deeply understand and improve the characteristics of MMCs. Xiao et al. [12] have studied the influence of an annealing step in N_2 atmosphere with WS_2 content up to 40 vol %. They observed a more pronounced decomposition of the lubricant phase and the undesired formation of copper sulfide (Cu_2S) when the applied annealing temperature is raised from 700 to 950 °C. Moreover, they measured an enhancement in composites' hardness from 75.4 HV of pure copper to 94.7 HV, promoted by a larger lubricant concentration. This behavior is opposite with respect to other species, such as graphite [36], as they generally entail an MMC softer than the virgin metal. Zhao et al. [37] have determined the effectiveness of WS_2 in strongly reducing the friction coefficient and the specific wear rate in copper-based composites, up to 0.16 and 5×10^{-5} mm^3 N^{-1} m^{-1} respectively. Jazaa et al. [38] have established that the reduction of WS_2 nanoparticles agglomeration and the enhancement of their dispersion in a polyalphaolefin (PAO) matrix do not substantially impact on the friction and wear minimization.

Rapoport et al. [39] have impregnated various densified solid porous matrices, prepared by means of PM, with IF nanoparticles. According to the experimental results on these composites, they have proposed a multiscale tribological model which is composed of two stages. In the first stage, IF nanoparticles reside in the pores. In the second one, they are slowly supplied to the metal surface where they act both as a lubricant and a spacer, alleviating wear damages and friction losses. Sade et al. [40] have tested inorganic fullerene-like WS_2 nanoparticles coated with a humin-like shell as additives in polyalphaolefin-4 (PAO-4) to reduce friction problems, observing that the presence of pre-exfoliated sheets facilitates the formation of the tribo-film while the coating fosters a better penetration into the tribological interface.

Guo et al. [41] have performed wear tests in a four-ball assembly on a polyalphaolefin-2 (PAO-2) oil enriched with multi-layered graphene, measuring a 78%-reduction of the friction coefficient and a beneficial reduction of wear rate. Pape et al. [42] have employed 1 wt % of graphene platelets with different thicknesses (2, 6–8, 11–15 nm) as dry lubricants and as additives in greases for rolling contacts operating under reciprocating motion. They have concluded that the excellent wear resistance and friction coefficient reduction are associated to the platelets covering the surface asperities and generating favorable sliding planes, although thickness seemed to not influence the performances.

To satisfy the increasingly demanding requirements of sliding electrical contacts for aerospace applications, Qian et al. [43] have fabricated hot-pressed MMCs consisting of a copper matrix, WS_2 and natural flake graphite at different concentrations. The studied materials displayed a good electrical sliding wear behavior, correlated to the simultaneous presence of the two lubricating agents. A positive synergistic effect is activated: graphite can act as oxygen diffusion barrier and as moisture scavenger, reducing WS_2 oxidation and improving sliding performances in medium-to-high humidity conditions; on the contrary, WS_2 is the main lubricating agent when vacuum conditions are applied. The further addition of 5 wt % WS_2 nanotubes [44] led to a denser microstructure, better electrical conductivity, higher hardness and higher elastic modulus than the Cu-WS_2-graphite samples. Besides, the authors have observed how WS_2 nanostructures can greatly limit both contact resistance and wear rate. This behavior has been attributed to the gradual detachment of WS_2 nanotubes from the brush surface and their adhesion to the frictional interface, where they can carry out their specific lubrication mechanism.

Despite WS_2, IF nanoparticles and GNP can offer many advantages as solid lubricants, their large-scale application is still not very widespread, therefore further insights are mandatory.

This study preliminarily investigates the effects of different lubricants' contents and combinations on the tribological and electrical performances of self-lubricating copper-based composites. The aim is to identify a suitable design of these materials able to minimize the depletion of the components in sliding electrical contacts employed in the aerospace sector, which work under harsh conditions: outside temperature decreasing by approximately 2 °C per thousand feet, relative humidity up to 99% [45], and severe ice formation at low temperatures [46]. High electrical conductivity, hydrophobicity, and wear resistance are therefore required. The samples have been prepared via PM, which has been chosen due to its affordability and process simplicity. The metal matrix and the lubricants have been firstly mixed, ground, and homogenized in a ball milling system. Then, milled powders have been compacted in tablets via a cold-pressing technique. In the end, solid-state pressureless sintering has allowed to complete the procedure and achieve better mechanical features. Five different samples have been studied, the first two of which were made up of not-milled and 2-h ball milled pure copper, respectively. They have been considered as benchmarks. The third one contained 10 wt % of WS_2, whereas the others were manufactured combining WS_2 with IF-WS_2 nanoparticles and both IF and GNP, respectively. The fabricated composites have been extensively analyzed by means of X-ray diffraction (XRD), static optical contact angle (OCA) measurements, density evaluation, electrical properties assessment, indentation hardness tests, micro-scratch tests, and wear tests, in order to ascertain their wettability, electrical resistivity, mechanical, and tribological properties.

2. Materials and Methods

2.1. Materials

Makin Metal Powders, Rochdale, UK has provided electrolytic copper powders with a nominal particle size of 45 μm and a purity level > 99.5%. WS_2 micro-powders with a mean particle size of 2 μm and a purity of 99% have been purchased from Sigma-Aldrich Corporation, St. Louis, MO, USA. ACS Materials®, Pasadena, CA, USA, has supplied GNP with a nominal thickness of 2–10 nm and a purity > 99%. IF tungsten disulfide particles

have been obtained through a bulk synthesis route analogous to the one developed by Feldman et al. [25,26]. Tungsten trioxide (WO_3) micro-powders with a particle size $\leq$ 25 µm and a purity $\geq$ 99%, supplied from Sigma-Aldrich Corporation, St. Louis, MO, USA, have undergone a ball milling process for one week to further reduce their nominal dimension. Afterwards, they have been introduced in an EHA Model Carbolite-Gero, Hope, UK, 1200 °C E-Range Tube Furnace, equipped with a thermocouple and two Brooks® Instrument, Hatfield, PA, USA, Smart Mass Flow Controller 5850. Reagent grade sulfur (S) powder, as well acquired from Sigma-Aldrich Corporation, St. Louis, MO, USA, has been added to achieve a 1-to-3 weight ratio between WO_3 and S, specifically selected to guarantee an adequate sulfur content. Process temperature has been fixed to 850 °C to sublime the sulfur powder, whereas the reaction atmosphere has been controlled by a 95% N_2/5% H_2 gaseous stream to ensure a reducing environment. These conditions have allowed a first reduction of the outer layer of WO_3 particles to form a reaction intermediate, whose size has directly determined the final dimensions of the IF nanoparticles. A subsequent one-hour solid-state diffusion step has completed the sulfurization process and the nesting of IF structures until total consumption of sulfur.

Cu powders have been subjected to a preliminary oven-drying step at 120 °C for 6 h to eliminate residual moisture. Mixing and grinding of appropriate quantities of powders have been carried out via a 1-level roller ball milling system provided by MGS S.r.l., Olginate, Italy, with the aim of reducing particles dimension and obtaining a homogenous dispersion. In detail, powders and zirconia (ZrO_2) spheres with a 15-mm diameter have been inserted in a polyethylene (PE) container at a controlled 10-to-1 ball-to-powder (BPR) weight ratio. The container has been in turn introduced in a cylindrical porcelain alumina jar rolling on the mill at 60 rpm. Ball milling time has been fixed to 2 h. An ensuing cold-pressing technique has been performed to achieve powder compaction and tableting. A 6 tons-pressure has been applied by means of a Specac Ltd., Orpington, UK, hydraulic press for five minutes on a steel tablet-making device filled with 1.5 g of milled powder. The obtained tablets, connoted by a 13 mm-diameter and a thickness of roughly 2 mm, have undergone a sintering process in the EHA Tube Furnace under a controlled flow atmosphere of 95% N_2 and 5% H_2. A heating rate of 8 °C min^{-1} has been adopted up to a temperature of 550 °C. This upper limit has been chosen to prevent thermal decomposition of WS_2, observed in previous thermogravimetric analyses on pristine powders. The temperature has been maintained for one hour, before naturally cooling down the samples in the process environment.

A first pure copper specimen, referred to as Cu, has been prepared by directly proceeding with cold-pressing and sintering. Differently, the second copper sample has undergone the milling step, therefore it has been labelled as Cu-2. Then, three composites have been prepared mixing copper powder with different contents of lubricant phases. They have been produced to determine the improvements generated by the addition of solid lubricants in the copper matrix. The one named Cu-WS_2 has been fabricated with 10 wt % WS_2. The sample called Cu-WS_2-IF has been manufactured combining 10 wt % WS_2 with 5 wt % of previously synthesized IF nanoparticles. The last one, named Cu-WS_2-IF-GNP, has been obtained by adding 0.5 wt % GNP while maintaining the same content of WS_2 and IF.

2.2. X-ray Diffraction Analysis

The diffractometer D8 Advance by Bruker Corporation, Billerica, MA, USA, has allowed to execute X-ray diffraction (XRD) experiments. It has employed a Cu-Kα filament to emit X-rays with a wavelength of 1.54 Å. The operating parameters have been a scanning rate of 0.02° per second in the angular interval of 5–90°, an applied tension of 40 kV, an applied current of 40 mA and a count time of one second.

2.3. Optical Contact Angle Measurements

Static optical contact angle (OCA) measurements have been obtained by means of the OCA 15plus provided by DataPhysics Instruments GmbH, Filderstadt, Germany, implementing a sessile drop method. The instrument has been equipped with a 752 × 582 pixel-resolution CCD video-camera and supported by the image processing software SCA 20.

2.4. Density Measurements

The hydrostatic balance YDK01 by Sartorius AG, Göttingen, Germany, has enabled to weigh the specimens both in air and in water, in order to perform density assessments. The Archimedes' principle has been exploited to calculate the absolute density of the composites, identified as δ (g cm^{-3}), through Equation (1)

$$\delta = \frac{m_a \cdot \delta_w}{m_a - m_w} \quad (1)$$

in which m_a is the mass in air (g), δ_w is the density of water (g cm^{-3}) and m_w is the mass of the solid completely immersed in the solvent (g). The corresponding relative densities (δ_r, %) of the samples have been derived via Equation (2)

$$\delta_r = 100\frac{\delta}{\delta_{Cu}} \quad (2)$$

where δ_{Cu} is the tabulated density of pure copper, equal to 8.96 g cm^{-3} [47].

2.5. Electrical Properties Evaluation

Electrical resistance of each sample has been measured via the DC resistance-meter model 2841 supplied by B&K Precision Corporation, Yorba Linda, CA, USA, with a maximum accuracy of 0.01%. Two different experimental configurations have been chosen to minimize the dependence of the resistance outcomes to the geometrical conformation of the analyzed composites. In the first one, test clips have been arranged at the maximum distance, on the opposite sides of the tablet. The second one has been attained by placing one clip on the mid-section of the sample, while leaving the other one on the edge. The corresponding electrical resistivity ρ (Ω m) has been computed through the second Ohm's law, reported in Equation (3)

$$\rho = \frac{R \cdot t \cdot l}{d} \quad (3)$$

in which R is the assessed resistance (Ω), t is the thickness of the tablet (m), l is the length (m) of the chord perpendicular to the inter-distance, d (m), and placed halfway between the two clips (Figure 1). The geometrical parameters have been manually surveyed with a Fujisan digital micrometer, repeating each measurement three times to enhance the reliability of the results.

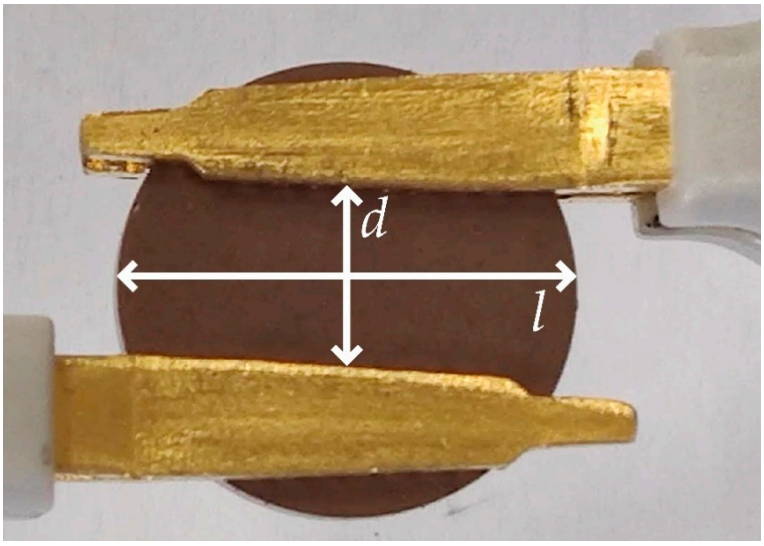

Figure 1. Geometrical parameters representation in electrical resistivity tests.

2.6. Tribological Analysis

Micro-scratch tests have been performed through the Micro-Scratch Tester provided by CSM Instruments SA, Needham, MS, USA. The instrument has exploited a conical Rockwell stainless steel indenter model V-227, having a 200 µm-radius spherical diamond tip. The procedure has consisted of a pre-scan, an actual scratch stage and a post-scan. The pre-scan stage has allowed the evaluation of the surface profile of the sample by sliding the indenter at the lowest normal load (0.03 N). The actual scratch stage has enabled to record the evolution of the actual normal force (F_n, N), the actual tangential force (F_t, N) and the penetration depth (P_d, mm) by applying a nominal normal load of 15 N at a constant speed of 20 mm min^{-1} for a 5 mm-distance. A total of ten scratches have been incised on each specimen, from which six suitable measurements have been selected by discarding the off-scale values. During the post-scan, the topography of the damaged area has been scanned to evaluate the residual depth (R_d, mm). Several mechanical features have been determined combining the parameters directly acquired from the experiments. Equation (5) has permitted to estimate the friction coefficient (FC) as the ratio between the actual tangential force and the actual normal force

$$FC = \frac{F_t}{F_n} \tag{4}$$

Scratch hardness (H_s, MPa) has been derived via Equation (6) as the ratio between the actual normal force and the contact area (A_c, mm^2)

$$H_s = \frac{F_n}{A_c} \tag{5}$$

Contact area has been assumed as half of the circular projection left on the specimen by the indenter's spherical tip. The radius of the projection has been considered as half of the residual width.

The TECMET 2000 S.r.l., Corsico, Italy, Microhardness Tester FM700, comprising a square pyramid-shaped indenter with an angle (θ) of 136° between the opposite faces, has been employed to carry out indentation hardness tests. Vickers hardness (HV) values have been extrapolated via Equation (4) as average of three different estimations, considering the applied load (P) of 0.5 kg and the average length (L) of the diagonal left by the indenter on the samples (mm)

$$HV = \frac{2 \cdot P \cdot \sin\left(\frac{\theta}{2}\right)}{L^2} \tag{6}$$

The CSM Instruments SA, Needham, MS, USA, tribometer has permitted the execution of wear tests with a ball-on-disk configuration under room temperature and atmosphere. A 100Cr6 steel counter ball, characterized by a diameter of 6 mm and a hardness of 831 ± 21 HV, has been chosen to effectively etch the softer copper-based composites while avoiding an excessive deformation or their complete destruction. A nominal normal load of 5 N has been applied on the counter ball. The tablets have been fastened to a mandrel and rotated at a controlled tangential speed of 0.18 m s^{-1}, in order to let the counter ball cover an overall distance of 500 m. The evolution of the friction coefficient has been recorded as a function of the run distance to deduce the wear behavior of the prepared materials. Samples' wear tracks and worn counter balls have been inspected with the optical microscope (OM) Nikon, Tokyo, Japan, Eclipse LV150NL. Scanning electron microscopy (SEM) images of the wear tracks of the composites (Cu-WS_2, Cu-WS_2-IF, and Cu-WS_2-IF-GNP) have been acquired by the Cambridge Scientific Instrument Company, London, UK Stereoscan 360 at 400× and 1500× magnifications.

3. Results

3.1. X-ray Diffraction

The two samples of pure copper Cu and Cu-2, black and red line respectively in Figure 2, show as expected only typical Cu peaks: at about 43° for Cu (1 1 1), at 50° for Cu (2 0 0), and at 74° for Cu (2 2 0). The samples containing solid lubricants, Cu-WS_2 (blue), Cu-WS_2-IF (green), and Cu-WS_2-IF-GNP (purple), exhibit the same peaks for copper and the characteristic peaks of tungsten disulfide that are 14° for WS_2 (0 0 2), 29° for WS_2 (0 0 4), 44° for WS_2 (0 0 6), and 60° for WS_2 (0 0 8) [48–54]. The peak usually observable in the range 24°–26°, related to the presence of graphene [55], is not detected in the sample Cu-WS_2-IF-GNP.

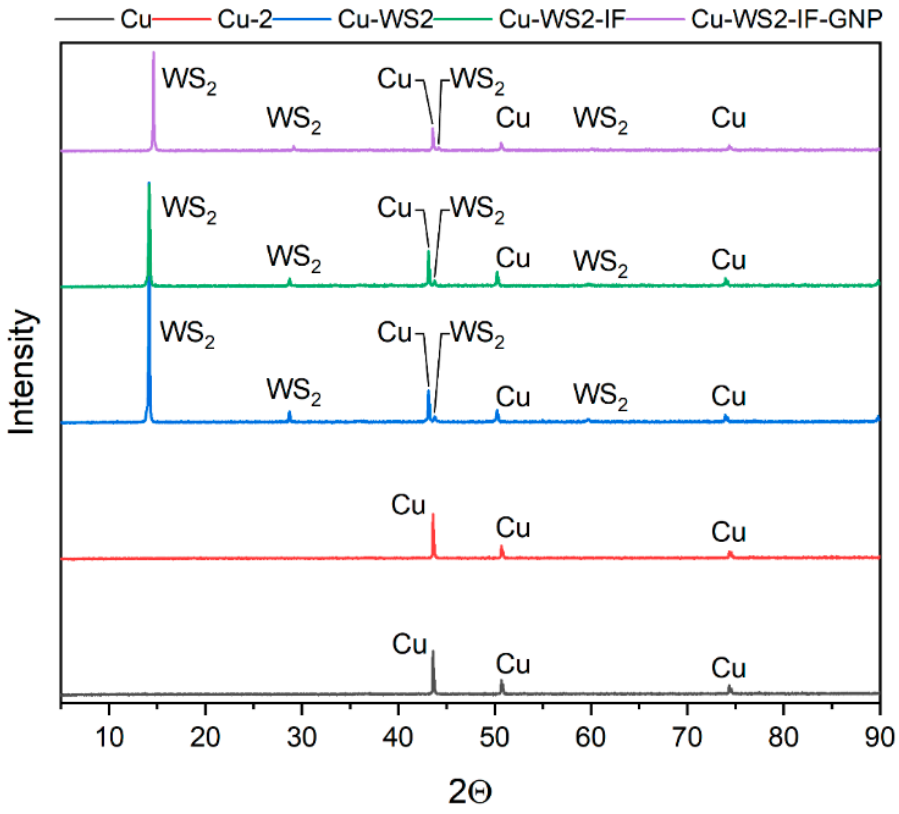

Figure 2. X-ray diffraction analysis results of pure copper and copper matrix composites.

3.2. Optical Contact Angle

The investigation of the wettability properties highlights a general hydrophobic behavior for both pure copper and copper matrix composites samples. The results are reported in Figure 3, in which the hydrophobic threshold at 90° is depicted. The detailed values are listed in Table 1, as well as the corresponding standard deviations obtained from 10 different measurements executed on each sample. Figure 4 portrays 3 µL-drops lying on the samples' surfaces after being released from the needle tip of the Hamilton syringe. Contact angles range from 115.7° of the sample Cu-2 to 137.5° of the sample Cu-WS_2-IF. Pure copper samples have almost identical values, in the neighborhood of 115°. The introduction of WS_2 produces an increase of the contact angle leading to an even more hydrophobic behavior. The combination with IF provokes a further increase of the contact angle up to 137.5°, whereas the addition of GNP causes a slight decrease up to 123.2°. Despite Cu-2 and Cu-WS_2-IF-GNP are characterized by a high standard deviation, the small variability of the other sample suggests an acceptable homogeneity.

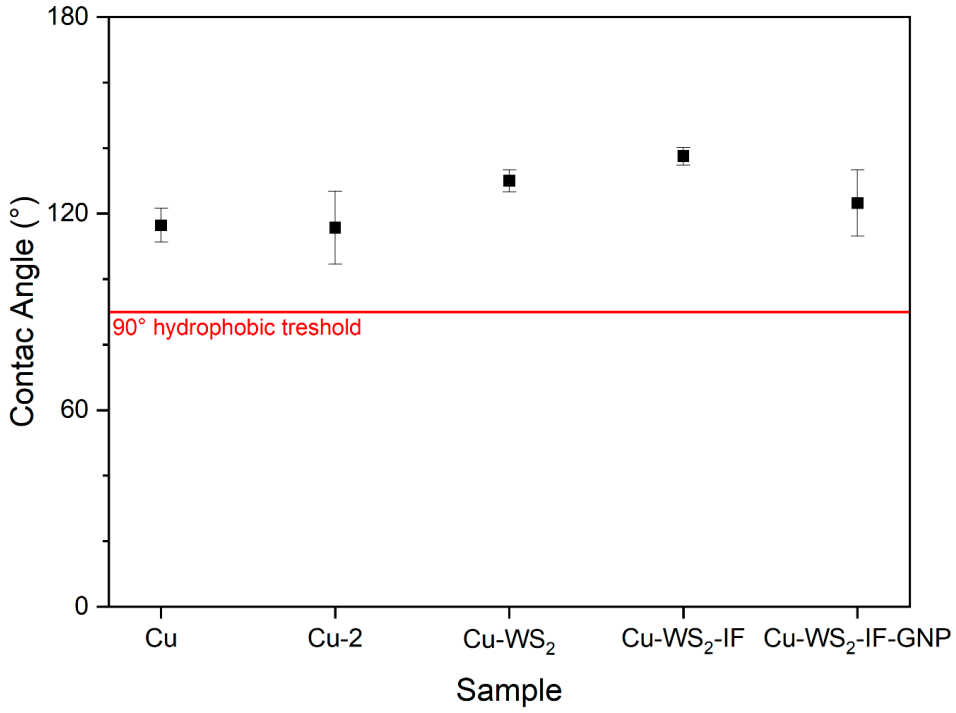

Figure 3. Optical contact angle results of pure copper and copper matrix composites.

Table 1. Mean optical contact angle values and corresponding standard deviations of pure copper and copper matrix composites

OCA	Mean Value (°)	Standard Deviation
Cu	116.4	5.2
Cu-2	115.7	11.2
Cu-WS_2	130.0	3.4
Cu-WS_2-IF	137.5	2.7
Cu-WS_2-IF-GNP	123.2	10.1

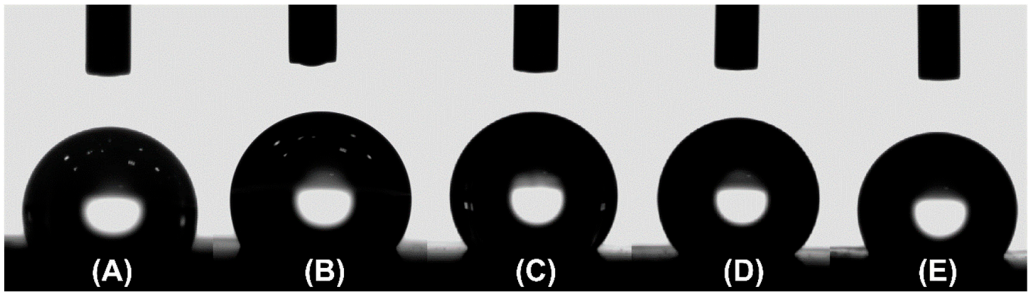

Figure 4. Water drops on (**A**) Cu, (**B**) Cu-2, (**C**) Cu-WS_2, (**D**) Cu-WS_2-IF, (**E**) Cu-WS_2-IF-GNP during optical contact angle measurements.

3.3. Relative Density

The results of the density measurements are listed in Table 2. The outcomes of produced samples highlight the presence of a residual internal micro- or macro- porosity. The recorded densities are quite similar for all the samples, recommending the consistency and reproducibility of the production method. Considering that the total percentage of the lubricant phases is 15 wt % and 15.5 wt % for Cu-WS_2-IF and Cu-WS_2-IF-GNP respectively, and that the introduced nanostructured materials are connoted by low density and a hollow architecture, the density decrease can be considered reliable.

Table 2. Relative densities outcomes of pure copper and copper matrix composites.

Relative Density	Value (%)
Cu	86.29
Cu-2	85.83
Cu-WS_2	85.36
Cu-WS_2-IF	83.23
Cu-WS_2-IF-GNP	81.61

3.4. Electrical Resistivity

The mean electrical resistivity values of Cu and Cu-2 are higher with respect to the tabulated value of pure copper, 1.68×10^{-8} Ω m [47]. A possible explanation is the presence of impurities in the copper powder, although limited; moreover, the residual porosity due to the production method penalizes the connection between the powder grains. As reported in Table 3, the introduction of WS_2 increases the electrical resistivity due to its insulating behavior. It should be noticed that the 10 wt %-amount of solid lubricant, which has been found as the optimum in previous research of this group, determines a value that remains in the same order of magnitude of copper samples and of pure copper itself; a high electrical conductivity is therefore preserved.

Table 3. Mean electrical resistivity values and corresponding standard deviations of pure copper and copper matrix composites

Electrical Resistivity	Mean Value (Ω m)	Standard Deviation
Cu	2.96×10^{-8}	1.45×10^{-9}
Cu-2	3.00×10^{-8}	5.28×10^{-10}
Cu-WS_2	7.08×10^{-8}	9.28×10^{-10}
Cu-WS_2-IF	8.84×10^{-8}	3.31×10^{-8}
Cu-WS_2-IF-GNP	9.33×10^{-8}	1.60×10^{-8}

3.5. Micro-Scratch Test

As previously discussed, the micro-scratch test outputs are the tangential and normal forces, the penetration depth, and the residual depth, recorded pointwise by the instrumentation during the test. A total of 10 tests have been carried out on each sample, and,

from Equations (4) and (5), the mean friction coefficient and scratch hardness have been calculated. Figure 5 shows the mean friction coefficients evaluated for pure copper and composite materials samples. The 2-h ball milling causes a higher friction coefficient with respect to the sample made of pristine copper powder, from 0.441 to 0.603. On the other hand, friction coefficient is lessened by the introduction of solid lubricants, that enable reaching values below 0.360. The best performance is exhibited by Cu-WS_2-IF, whose friction coefficient is 0.304.

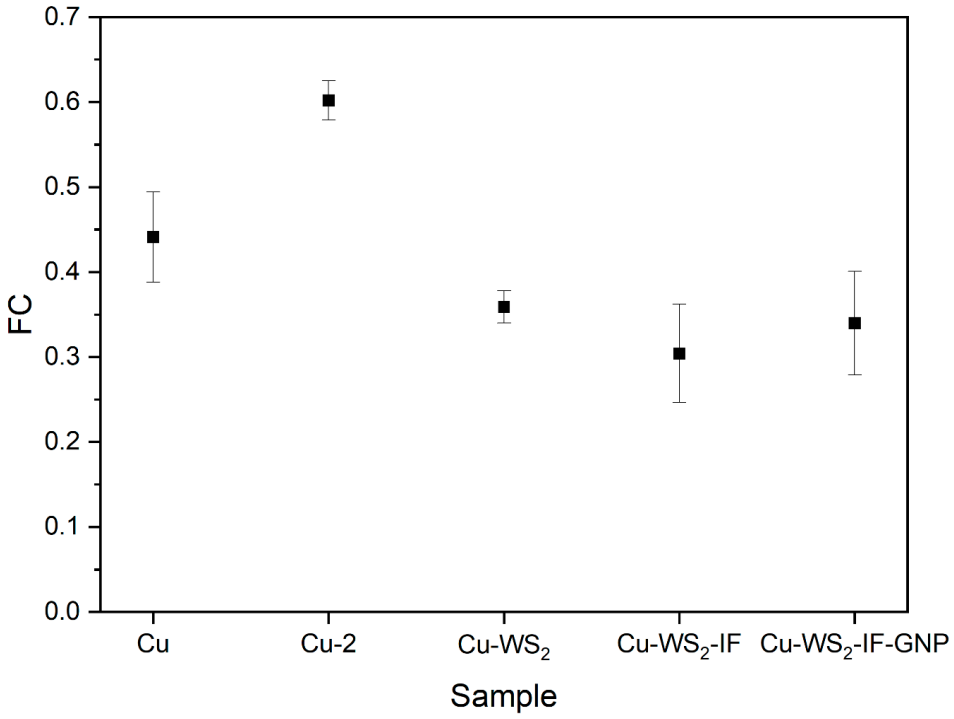

Figure 5. Friction coefficient values of pure copper and copper matrix composites.

Scratch hardness outcomes are presented in Figure 6. Milling of copper powder leads to a slight increase of the scratch hardness from 654.8 MPa to 672.1 MPa with respect to unmilled copper, thanks to a smaller and more homogeneous size of the powder. The strengthening effect of WS_2 reported by Xiao et al. [12] is confirmed in this study; the addition of 10 wt % of WS_2 improves the scratch hardness from 672.1 MPa to 787.9 MPa. The presence of IF nanostructures in Cu-WS_2-IF diminishes the scratch hardness up to 543.0 MPa, while the further addition of GNP does not involve relevant variations. The values and the corresponding standard deviations of friction coefficient and scratch hardness of pure copper and copper matrix composites are recapitulated in Table 4.

Table 4. Mean values and corresponding standard deviations of micro-scratch test outputs.

Micro-Scratch Test	Friction Coefficient	Standard Deviation	Scratch Hardness (MPa)	Standard Deviation
Cu	0.441	0.053	654.8	91.4
Cu-2	0.603	0.023	672.1	25.2
Cu-WS_2	0.359	0.019	787.9	66.6
Cu-WS_2-IF	0.304	0.058	543.0	31.3
Cu-WS_2-IF-GNP	0.340	0.061	526.9	55.9

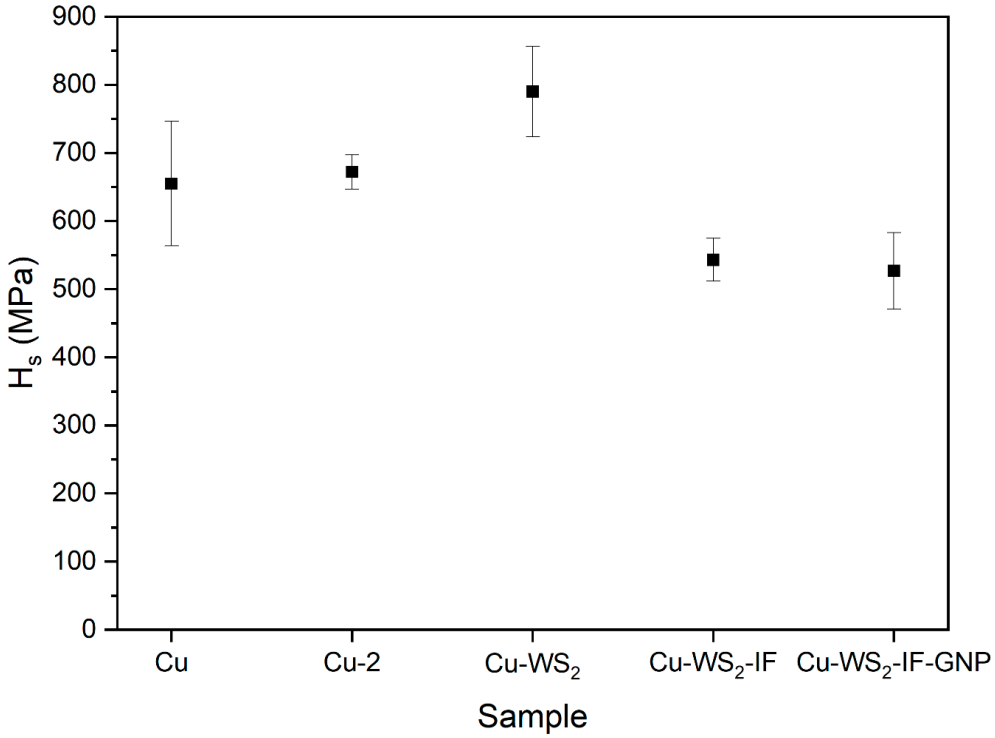

Figure 6. Scratch hardness values of pure copper and copper matrix composites.

3.6. Indentation Hardness

Table 5 collates Vickers hardness values of pure copper and copper matrix composites, extrapolated via Equation (6) from indentation hardness tests. Outcomes of the two copper samples are quite similar, 55.0 and 57.5 HV. As similarly observed from micro-scratch tests, the introduction of WS_2 leads to a hardening effect, allowing Cu-WS_2 to exhibit the highest value recorded in this study, 71.0 HV. A reduction of Vickers hardness is found with the succeeding addition of nanostructured materials. Anyhow, the values of the Cu-WS_2-IF and Cu-WS_2-IF-GNP are higher than those of the copper samples.

Table 5. Mean Vickers hardness values and corresponding standard deviations of pure copper and copper matrix composites

Vickers Hardness	Mean Value (HV)	Standard Deviation
Cu	55.0	2.9
Cu-2	57.5	0.2
Cu-WS_2	71.0	1.5
Cu-WS_2-IF	60.9	0.9
Cu-WS_2-IF-GNP	63.6	3.9

3.7. Wear Test

The results of the wear tests, performed with a tangential speed of 0.18 m s^{-1} and a normal load of 5 N for 500 m, are shown in Figure 7. The friction coefficient is reported for all the investigated samples as a function of the covered distance: Cu (black curve), Cu-2 (red curve), Cu-WS_2 (blue curve), Cu-WS_2-IF (green curve), and Cu-WS_2-IF-GNP (purple curve). The test of Cu (black curve) stopped after approximately 100 m due to high friction. For Cu-2 (red curve), the evolution of the friction coefficient exhibits two steps, the first one at 20 m and the second one at 50 m, after which a plateau of 0.75 is reached. The presence of solid lubricants in the prepared composites, Cu-WS_2 (blue curve), Cu-WS_2-IF (green curve), and Cu-WS_2-IF-GNP (purple curve) is immediately visible, as friction coefficient is strongly reduced and ranges between 0.12 and 0.18. Different behaviors are evident

considering the three composite samples. Cu-WS_2 (blue curve) shows a transition from 150 m to 200 m, where the friction coefficient decreases from 0.18 to 0.12; a similar drop is observed for Cu-WS_2-IF (green curve), albeit at a higher distance (420–450 m). Differently, Cu-WS_2-IF-GNP (purple curve) reaches a constant friction coefficient value, around 0.15, after the coupling of the two surfaces in the initial 20 m.

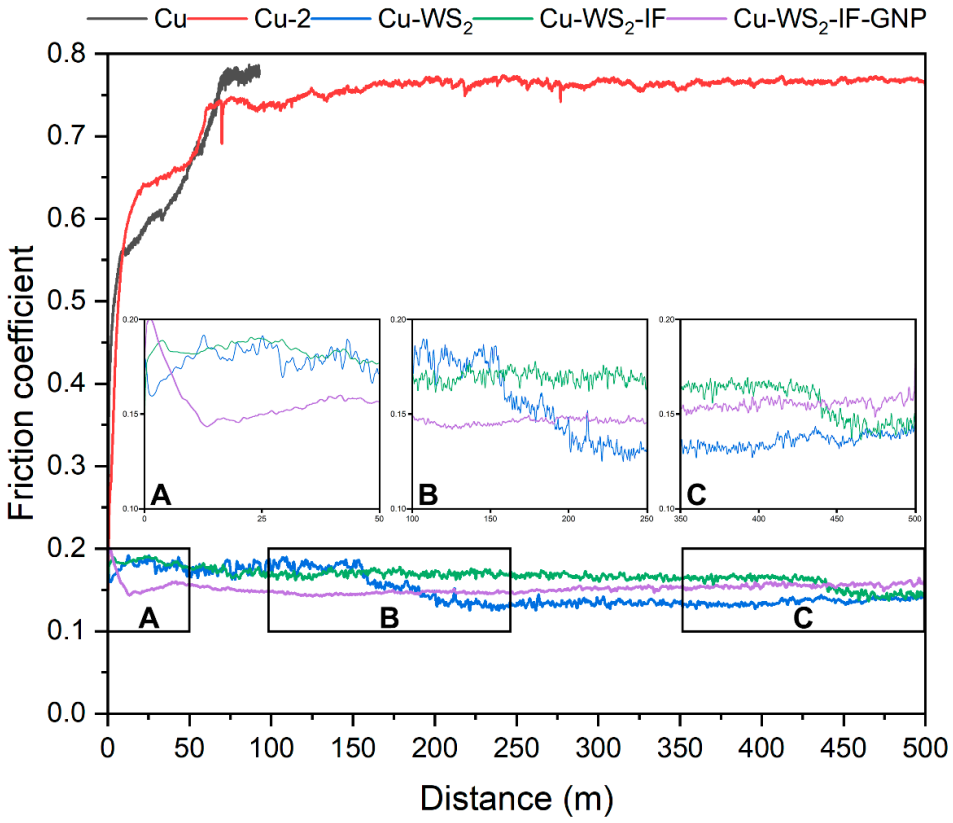

Figure 7. Friction coefficient analysis of pure copper and copper matrix composites from wear tests.

Figure 8 gathers the OM images of the wear tracks left on the samples Cu-2 (A), Cu-WS_2 (B), Cu-WS_2-IF (C), and Cu-WS_2-IF-GNP (D) at different magnifications, as well as the wear tracks of the corresponding counter balls. The analysis of the wear track widths, reported in Table 6, suggests the wear mechanisms occurred during tests. The 1141 µm-wide black spotted track of Cu-2 is taken as benchmark. An abrasive mechanism can be assessed for the investigated samples, due to all counter balls being worn-out. Cu-WS_2 higher hardness determines a more severe damage of the counter body, enlarging the contact area and leading to a wider wear track (1255 µm). The presence of IF nanoparticles in Cu-WS_2-IF inhibits the contact between the mating surfaces, decreasing both the wear of the counter ball and the span of the track (586 µm). The variable width of the wear track in Cu-WS_2-IF-GNP (330–841 µm) points out the presence of a third body that regularly outdistances the counter ball and the sample surface. Wear is consequently limited, but the correlated debris formation during sliding could cause undesired damage of the assembly, representing an important issue in sliding electrical contacts. Furthermore, the periodic outrun of the surfaces fosters the generation of electric arches which entail harsher damage of the components.

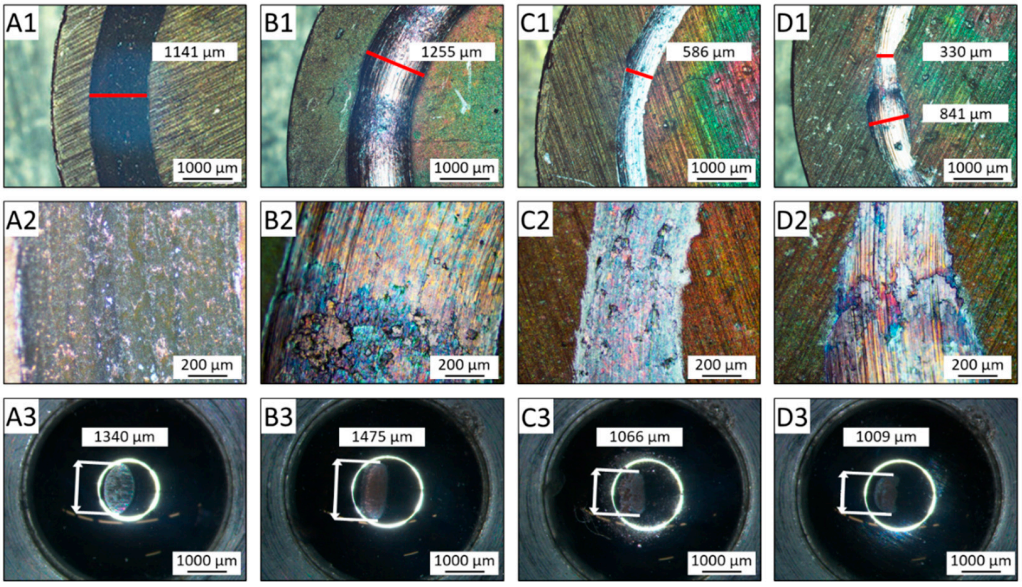

Figure 8. OM images of the wear tracks of Cu-2 at 25× (**A1**) and 50× (**A2**), Cu-WS_2 at 25× (**B1**) and 50× (**B2**), Cu-WS_2-IF at 25× (**C1**) and 50× (**C2**), Cu-WS_2-IF-GNP at 25× (**D1**) and 50× (**D2**), and of the counter balls of Cu-2 (**A3**), Cu-WS_2 (**B3**), Cu-WS_2-IF (**C3**), and Cu-WS_2-IF-GNP (**D3**) at 25× magnification.

Table 6. Wear track widths of tested samples and of the corresponding counter balls.

Wear Test	Wear Track Width (µm)	
	Sample	Counter Ball
(A) Cu-2	1141	1340
(B) Cu-WS_2	1255	1475
(C) Cu-WS_2-IF	586	1066
(D) Cu-WS_2-IF-GNP	330–841	1009

SEM images of the post-wear test composites are collected in Figure 9, in order to observe differences in the morphology of the worn surfaces. Cu-WS_2 (Figure 9A) appears to show an overall abrasive mechanism, with material removal throughout the wear track. A tribo-film promoted by the solid lubricant, spotted in the top-left corner, can be further appreciated at higher magnification. The presence of flattened and scaled debris may also imply the occurrence of an adhesive mechanism. Cu-WS_2-IF (Figure 9B) exhibits a smoother and more homogenous tribo-layer, thanks to the synergic effect of WS_2 and IF nanoparticles that permits to avoid an accentuated debris formation due to the counter ball sliding [56]. As already noticed by the optical microscopy (Figure 8D), the worn surface of Cu-WS_2-IF-GNP (Figure 9C) is more jagged and debris-rich, confirming a possible third-body mechanism that periodically enlarges the wear track and favors the accumulation of removed material.

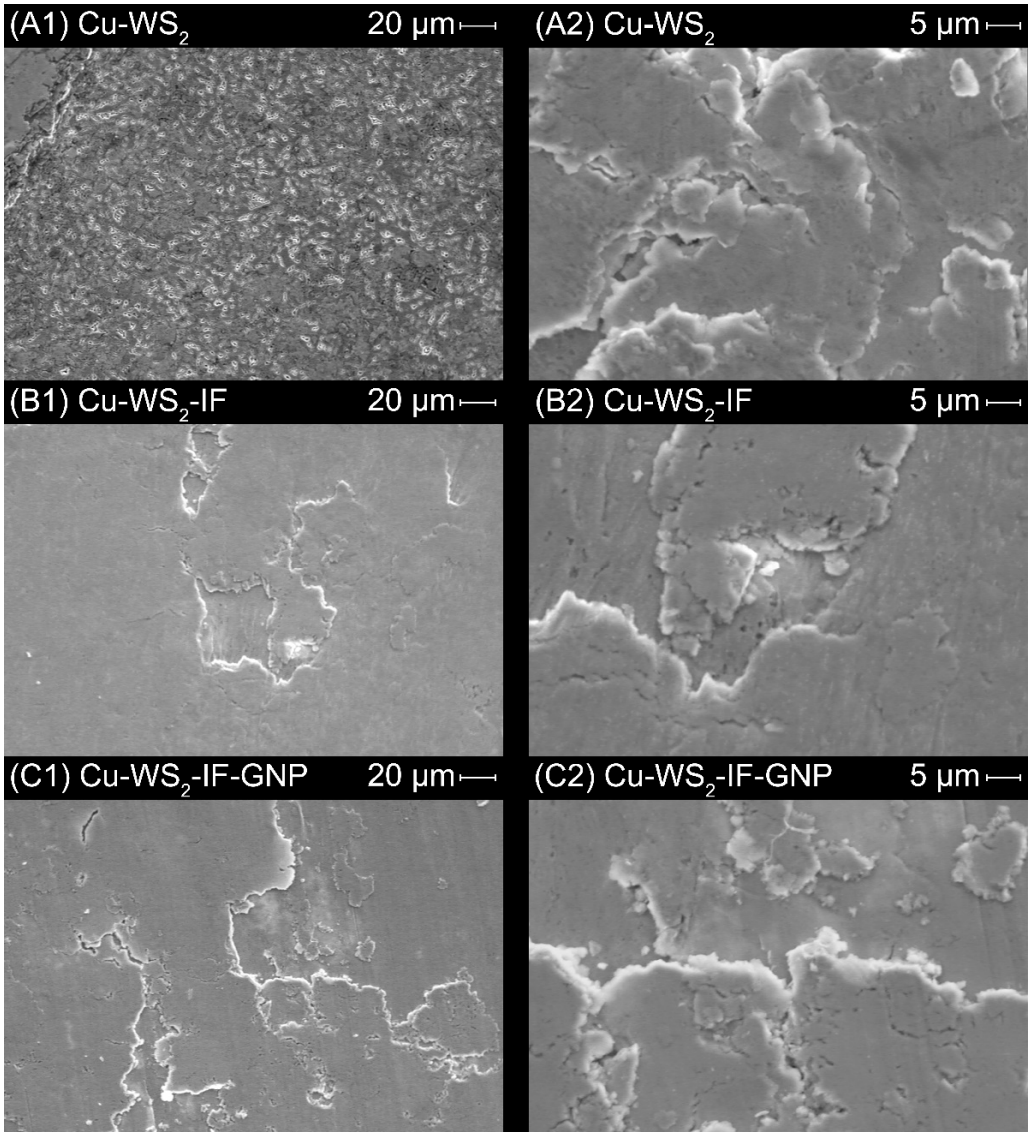

Figure 9. SEM images of the wear tracks of Cu-WS_2, Cu-WS_2-IF, and Cu-WS_2-IF-GNP at 400× (**A1**,**B1**,**C1**) and 1500× (**A2**,**B2**,**C2**) magnifications.

4. Discussion

The presented results demonstrate the reliability of the production method. XRD patterns highlight that no unwanted phases or compounds are produced during neither the ball milling nor the sintering process. In detail, Cu_2S formation due to the reaction of copper and tungsten disulfide is prevented, as the characteristic Cu_2S (2 0 3) peak at about 25.9° is not detected [12]. No decomposition occurs as well, since W peaks typically observable at 40° for W (1 1 0), 57° for W (2 0 0), and 72° for W (2 1 1) are not spotted [57,58]. The absence of a contribution associable to graphene in Cu-WS_2-IF-GNP may be addressed to the low percentage of GNP (0.5 wt %), which may imply a smaller intensity with respect to others and a probable hiding by background noise. Density assessment corroborates the steadiness of the production process since the obtained values are almost constant and the changes can be addressed to the different structure of the lubricating agents with respect to the copper matrix. Relative density values lower than 100% may be addressed to the difficult packing of the dendritic copper powder, that intrinsically leads to the presence of voids. It would be possible to raise the density of the investigated samples increasing pressure in the cold-pressing step or extending the sintering time. The increase of density could determine a decrease of the electrical resistivity

thanks to the greater free path available for the electrical current passage. Anyway, the resistivity values measured in the present study are in the same order of magnitude of pure copper found in literature (1.68×10^{-8} Ω m [47]), despite the introduction of an insulating phase. From the electrical performance standpoint, the prepared composites are suitable for the final aim of this project, that is to identify a durable material to be employed in sliding electrical contacts exposed to extreme conditions. In aerospace applications, these components are subjected to a wide range of temperature and relative humidity, hence a hydrophobic behavior is as much required to avoid the formation of a uniform ice-layer on their surface, preserving the integrity and the performance of the assembly during service. All the analyzed composites display an exacerbated hydrophobicity with respect to pure copper samples, with contact angles higher than 120°. A more pronounced surface roughness could be hypothesized to clarify the increase in contact angle [59]. The presence of hydrophobic WS_2 layers may influence the surface structure and the wettability of the composites, allowing water droplets to become quasi-spherical. This effect is even emphasized by IF nanoparticles, whose conformation probably induces a local surface deformation and a further corrugation [60]. The combination with GNP could bring about a slight flattening, due to graphene sheets placement between surface asperities.

Wear resistance is of paramount importance to guarantee the reliability of sliding electrical contacts over long periods without maintenance. As well described by the Archard's equation [61], hardness is strictly related to the wear behavior of a specific material. In this study, pure copper powders' ball milling does not negatively influence the hardness performance, as previously reported in Section 3.6. Therefore, milling and grinding can be considered suitable to homogenize grain size and distribution of the second phase without any drawback. Additionally, indentation hardness evaluation underlines the strengthening effect of WS_2. According to Xiao et al. [12], the anisotropic lamellar structure of WS_2 and the improved interfacial bonding strength between lubricant layers and copper matrix could promote a hardness amelioration with respect to pure copper. The further addition of IF nanoparticles could lead to agglomeration and a slightly worse Vickers hardness. Moreover, it has to be considered that the total amount of second phase in Cu-WS_2-IF and Cu-WS_2-IF-GNP (15 wt % and 15.5 wt %) is higher with respect to Cu-WS_2 (10 wt %), therefore a decrease in Vickers hardness is expected. Nevertheless, the reinforcing action of WS_2 is still observable considering benchmark Cu and Cu-2. Scratch hardness outcomes appear to confirm the beneficial strengthening effect of WS_2, the agglomeration issues of IF nanoarchitectures and, in a more noticeable fashion, the detrimental softening induced by a larger amount of second phase. The solid lubricants determine a visible lowering of the friction coefficient in the micro-scratch tests, ensuring a lower energy consumption, a restraint of possible local heating, and a minimization of surface damaging due to friction. It should be noticed that the friction coefficients calculated from micro-scratch tests are not comparable with the ones obtained from wear tests, due to differences in the setup: in the first case, no tribo-film forms during the incision of the sample and the counter surface is a stainless steel Rockwell indenter with a diamond tip; in the second case, the counter surface is a 100Cr6 sphere that passes several times on the same point, allowing the effective formation of a tribo-film so as to well enough simulate the typical operative conditions of sliding electrical contacts. The results of the wear tests show a strong reduction of the friction coefficient. The composite materials display similarities in the wear behavior; an abrasive mechanism is detected for all the composites, albeit some differences have to be highlighted. Nonetheless, the actual evaluation of the wear rate is not possible because of the counter ball's wear. As a consequence, the difference in weight of the samples before and after the test is null or even negative, and the volume of debris is not computable. Analyzing the friction coefficient evolution (Figure 7), Cu-WS_2 (blue curve) presents two different plateaus. The first one is given by the formation of an oxide layer on the surface, which is then removed. The subsequent temperature increase activates the lubricating effect of WS_2 layers, which permit a further reduction of the friction coefficient up to 0.12 and trigger an adhesive mechanism. Cu-WS_2-IF (green curve) exhibits a similar

friction coefficient trend and two plateaus as well, even though the transition is delayed. The IF nanoparticles' instant action partially separates the sliding surfaces, lowering their damage and preventing the formation of an oxide layer. In this way, the distance at which WS_2 layered structures perform their lubrication effect, further reducing friction coefficient up to 0.13, is lengthened. In the end, the friction coefficient transition of Cu-WS_2-IF-GNP (purple curve) at really short distance, around 20 m, denotes the intrinsic lubricating behavior of GNP which stabilizes the composite surface. The friction coefficient is stable at 0.15, even though a third-body mechanism is evident from the wear track. Despite the Vickers hardness of Cu-WS_2-IF-GNP is comparable to Cu-WS_2-IF, the scratch hardness value indicates the softening induced by the GNP introduction and explains the debris formation due to lower shear stress resistance.

5. Conclusions

The effects of WS_2 micro-powders, IF tungsten disulfide nanoparticles, and GNP on the wettability, electrical properties, and tribological performances of CuMCs were investigated. An unmilled (Cu) and a 2-h ball milled pure copper samples (Cu-2) were considered as benchamarks. XRD analysis, OCA measurements, density and electrical properties evaluation, micro-scratch, indentation hardness, and wear tests were executed. The experimental results illustrate the benefits of combining a copper matrix with solid lubricants. The employed preparation procedure is reliable, as no unwanted phases are detected. Hydrophobicity in the composites is even accentuated with respect to pure copper. Electrical resistivity is maintained in the same order of magnitude of pure copper, despite relative density evaluation hints the presence of voids. WS_2 promotes an evident hardness improvement. The higher weight amount of second phase in Cu-WS_2-IF and Cu-WS_2-IF-GNP negatively affects the mechanical properties. Wear behavior of the self-lubricating composites is enhanced, as friction coefficient is strongly reduced. The different action of solid lubricants is analyzed via wear test results, and an abrasive mechanism in mainly highlighted.

Considering the electrical properties, the hydrophobic behavior, and the tribological performance, the combination of the two different WS_2 structures, micro-powder, and inorganic fullerene-like nanoparticles, in Cu-WS_2-IF represents at the current state the most promising solution to be used in sliding electrical contacts.

Author Contributions: Conceptualization, M.F., N.L. and G.D.; Data curation, M.F., G.Z., N.L. and G.D.; Formal analysis, M.F.; Investigation, M.F., G.Z. and M.M.; Methodology, M.F., G.Z. and M.M.; Supervision, N.L. and G.D.; Validation, N.L. and G.D.; Writing—original draft, M.F. and M.D.V.; Writing—review and editing, M.F., M.D.V., M.M., N.L. and G.D. All authors have read and agreed to the published version of the manuscript.

Funding: This research received no external funding.

Institutional Review Board Statement: Not applicable.

Informed Consent Statement: Not applicable.

Data Availability Statement: Data is contained within the article.

Conflicts of Interest: The authors declare no conflict of interest.

References

1. Holmberg, K.; Erdemir, A. Influence of tribology on global energy consumption, costs and emissions. *Friction* **2017**, *5*, 263–284. [CrossRef]
2. Sawa, K.; Shobert, E. Sliding Electrical Contacts (Graphitic Type Lubrication). In *Electrical Contacts*; Slade, P.G., Ed.; CRC Press: Boca Raton, FL, USA, 2014; pp. 1041–1079, ISBN 9781315216829.
3. Moberly, L.E.; Johnson, J.L. Application in Space Environments. *IEEE Trans. Aerosp.* **1965**, *AS-3*, 252–257. [CrossRef]
4. Poljanec, D.; Kalin, M. Effect of polarity and various contact pairing combinations of electrographite, polymer-bonded graphite and copper on the performance of sliding electrical contacts. *Wear* **2019**, *426–427*, 1163–1175. [CrossRef]

5. Grandin, M.; Wiklund, U. Wear phenomena and tribofilm formation of copper/copper-graphite sliding electrical contact materials. *Wear* **2018**, *398–399*, 227–235. [CrossRef]
6. Bares, J.A.; Argibay, N.; Dickrell, P.L.; Bourne, G.R.; Burris, D.L.; Ziegert, J.C.; Sawyer, W.G. In situ graphite lubrication of metallic sliding electrical contacts. *Wear* **2009**, *267*, 1462–1469. [CrossRef]
7. Slade, P.G. (Ed.) *Electrical Contacts: Principles and Applications*, 2nd ed.; CRC Press: Boca Raton, FL, USA, 2014; ISBN 9781315216829.
8. Lince, J.R. Effective Application of Solid Lubricants in Spacecraft Mechanisms. *Lubricants* **2020**, *8*, 74. [CrossRef]
9. Vaziriserehk, M.R.; Martini, A.; Strubbe, D.A.; Baykara, M.Z. Solid lubrication with MOS_2: A review. *Lubricants* **2019**, *7*, 57. [CrossRef]
10. Natarajan, N.; Krishnaraj, V.; Davim, J.P. *Metal Matrix Composites Synthesis, Wear Characteristics, Machinability Study of MMC Brake Drum*; Springer: Berlin/Heidelberg, Germany, 2014; ISBN 9783319029849.
11. Sawa, K. Sliding Electrical Contacts and Materials. In *Encyclopedia of Tribology*; Wang, Q.J., Chung, Y.-W., Eds.; Springer: Boston, MA, USA, 2013; pp. 3133–3141, ISBN 978-0-387-92897-5.
12. Xiao, J.K.; Zhang, W.; Zhang, C. Microstructure evolution and tribological performance of Cu-WS_2 self-lubricating composites. *Wear* **2018**, *412–413*, 109–119. [CrossRef]
13. Selvi, E.; Ma, Y.; Aksoy, R.; Ertas, A.; White, A. High pressure X-ray diffraction study of tungsten disulfide. *J. Phys. Chem. Solids* **2006**, *67*, 2183–2186. [CrossRef]
14. Srivastava, S.K.; Avasthi, B.N. Layer type tungsten dichalcogenide compounds: Their preparation, structure, properties and uses. *J. Mater. Sci.* **1985**, *20*, 3801–3815. [CrossRef]
15. Wong, K.C.; Lu, X.; Cotter, J.; Eadie, D.T.; Wong, P.C.; Mitchell, K.A.R. Surface and friction characterization of MoS_2 and WS_2 third body thin films under simulated wheel/rail rolling-sliding contact. *Wear* **2008**, *264*, 526–534. [CrossRef]
16. Tenne, R.; Margulis, L.; Genut, M.; Hodes, G. Polyhedral and cylindrical structures of tungsten disulphide. *Nature* **1992**, *360*, 444–446. [CrossRef]
17. Margolin, A.; Deepak, F.L.; Popovitz-Biro, R.; Bar-Sadan, M.; Feldman, Y.; Tenne, R. Fullerene-like WS_2 nanoparticles and nanotubes by the vapor-phase synthesis of WCln and H2S. *Nanotechnology* **2008**, *19*. [CrossRef] [PubMed]
18. Rapoport, L.; Leshchinsky, V.; Lvovsky, M.; Nepomnyashchy, O.; Volovik, Y.; Tenne, R. Mechanism of friction of fullerenes. *Ind. Lubr. Tribol.* **2002**, *54*, 171–176. [CrossRef]
19. Rapoport, L.; Fleischer, N.; Tenne, R. Fullerene-like WS_2 nanoparticles: Superior lubricants for harsh conditions. *Adv. Mater.* **2003**, *15*, 651–655. [CrossRef]
20. Tevet, O.; Von-huth, P.; Popovitz-biro, R.; Rosentsveig, R.; Wagner, H.D.; Tenne, R. Friction mechanism of individual multilayered nanoparticles. *Proc. Natl. Acad. Sci. USA* **2011**, *108*, 19901–19906. [CrossRef]
21. Uflyand, I.E.; Zhinzhilo, V.A.; Burlakova, V.E. Metal-containing nanomaterials as lubricant additives: State-of-the-art and future development. *Friction* **2019**, *7*, 93–116. [CrossRef]
22. Erdemir, A. A crystal-chemical approach to lubrication by solid oxides. *Tribol. Lett.* **2000**, *8*, 97–102. [CrossRef]
23. Shalom, H.; Sui, X.M.; Elianov, O.; Brumfeld, V.; Rosentsveig, R.; Pinkas, I.; Feldman, Y.; Kampf, N.; Wagner, H.D.; Lachman, N.; et al. Nanocomposite of poly(L-lactic acid) with inorganic nanotubes of WS 2. *Lubricants* **2019**, *7*, 28. [CrossRef]
24. Kaplan-Ashiri, I.; Tenne, R. On the Mechanical Properties of WS_2 and MoS2 Nanotubes and Fullerene-Like Nanoparticles: In Situ Electron Microscopy Measurements. *JOM* **2016**, *68*, 151–167. [CrossRef]
25. Feldman, Y.; Frey, G.L.; Homyonfer, M.; Lyakhovitskaya, V.; Margulis, L.; Cohen, H.; Hodes, G.; Hutchison, J.L.; Tenne, R. Bulk synthesis of inorganic fullerene-like MS_2 (M = Mo, W) from the respective trioxides and the reaction mechanism. *J. Am. Chem. Soc.* **1996**, *118*, 5362–5367. [CrossRef]
26. Feldman, Y.; Lyakhovitskaya, V.; Tenne, R. Kinetics of nested inorganic fullerene-like nanoparticle formation. *J. Am. Chem. Soc.* **1998**, *120*, 4176–4183. [CrossRef]
27. Jang, B.Z.; Zhamu, A. Processing of nanographene platelets (NGPs) and NGP nanocomposites: A review. *J. Mater. Sci.* **2008**, *43*, 5092–5101. [CrossRef]
28. Hernandez, Y.; Nicolosi, V.; Lotya, M.; Blighe, F.M.; Sun, Z.; De, S.; McGovern, I.T.; Holland, B.; Byrne, M.; Gun'ko, Y.K.; et al. High-yield production of graphene by liquid-phase exfoliation of graphite. *Nat. Nanotechnol.* **2008**, *3*, 563–568. [CrossRef]
29. Cataldi, P.; Athanassiou, A.; Bayer, I.S. Graphene nanoplatelets-based advanced materials and recent progress in sustainable applications. *Appl. Sci.* **2018**, *8*, 1438. [CrossRef]
30. Jiménez-Suàrez, A.; Prolongo, S.G. Graphene Nanoplatelets. *Appl. Sci.* **2020**, *10*, 1753. [CrossRef]
31. Saboori, A.; Dadkhah, M.; Fino, P.; Pavese, M. An overview of metal matrix nanocomposites reinforced with graphene nanoplatelets; mechanical, electrical and thermophysical properties. *Metals* **2018**, *8*, 423. [CrossRef]
32. Zhang, D.; Zhan, Z. Preparation of graphene nanoplatelets-copper composites by a modified semi-powder method and their mechanical properties. *J. Alloys Compd.* **2016**, *658*, 663–671. [CrossRef]
33. Tabandeh-Khorshid, M.; Kumar, A.; Omrani, E.; Kim, C.; Rohatgi, P. Synthesis, characterization, and properties of graphene reinforced metal-matrix nanocomposites. *Compos. Part B Eng.* **2020**, *183*, 107664. [CrossRef]
34. Bonse, J.; Koter, R.; Hartelt, M.; Spaltmann, D.; Pentzien, S.; Höhm, S.; Rosenfeld, A.; Krüger, J. Femtosecond laser-induced periodic surface structures on steel and titanium alloy for tribological applications. *Appl. Phys. A Mater. Sci. Process.* **2014**, *117*, 103–110. [CrossRef]

35. Gnilitskyi, I.; Rota, A.; Gualtieri, E.; Valeri, S.; Orazi, L. Tribological properties of high-speed uniform femtosecond laser patterning on stainless steel. *Lubricants* **2019**, *7*, 83. [CrossRef]
36. Xiao, J.K.; Zhang, L.; Zhou, K.C.; Wang, X.P. Microscratch behavior of copper-graphite composites. *Tribol. Int.* **2013**, *57*, 38–45. [CrossRef]
37. Zhao, L.; Yao, P.; Gong, T.; Zhou, H.; Deng, M.; Wang, Z.; Zhang, Z.; Xiao, Y.; Luo, F. Effect of Adding Tungsten Disulfide to a Copper Matrix on the Formation of Tribo-Film and on the Tribological Behavior of Copper/Tungsten Disulfide Composites. *Tribol. Lett.* **2019**, *67*, 98. [CrossRef]
38. Jazaa, Y.; Lan, T.; Padalkar, S.; Sundararajan, S. The effect of agglomeration reduction on the tribological behavior of WS_2 and MoS2 nanoparticle additives in the boundary lubrication regime. *Lubricants* **2018**, *6*, 106. [CrossRef]
39. Rapoport, L.; Lvovsky, M.; Lapsker, I.; Leshinsky, V.; Volovik, Y.; Feldman, Y.; Zak, A.; Tenne, R. Slow release of fullerene-like WS_2 nanoparticles as a superior solid lubrication mechanism in composite matrices. *Adv. Eng. Mater.* **2001**, *3*, 71–75. [CrossRef]
40. Sade, H.; Moshkovich, A.; Lellouche, J.P.; Rapoport, L. Testing of WS_2 nanoparticles functionalized by a humin-like shell as lubricant additives. *Lubricants* **2018**, *6*, 3. [CrossRef]
41. Guo, Y.B.; Zhang, S.W. The tribological properties of multi-layered graphene as additives of PAO_2 oil in steel-steel contacts. *Lubricants* **2016**, *4*, 30. [CrossRef]
42. Pape, F.; Poll, G. Investigations on graphene platelets as dry lubricant and as grease additive for sliding contacts and rolling bearing application. *Lubricants* **2020**, *8*, 3. [CrossRef]
43. Qian, G.; Feng, Y.; Chen, Y.M.; Mo, F.; Wang, Y.Q.; Liu, W.H. Effect of WS_2 addition on electrical sliding wear behaviors of Cu-graphite-WS_2 composites. *Trans. Nonferrous Met. Soc. China* **2015**, *25*, 1986–1994. [CrossRef]
44. Qian, G.; Feng, Y.; Chen, F.; Liu, W.; Zhang, X.; Liu, Y. Effect of current polarity on electrical sliding wear behavior of Cu-WS_2-graphite-WS_2 nanotube composites in air and vacuum conditions. *Sci. China Technol. Sci.* **2013**, *56*, 2839–2846. [CrossRef]
45. Federal Aviation Administration. *Pilot's Handbook of Aeronautical Knowledge*; Federal Aviation Administration: Washington, DC, USA, 2016; p. 524.
46. Alemour, B.; Badran, O.; Hassan, M.R. A review of using conductive composite materials in solving lightening strike and ice accumulation problems in aviation. *J. Aerosp. Technol. Manag.* **2019**, *11*, 1–23. [CrossRef]
47. Haynes, W.M. *CRC Handbook of Chemistry and Physics*; Haynes, W.M., Lide, D.R., Bruno, T.J., Eds.; CRC Press: Boca Raton, FL, USA, 2016; ISBN 9781315380476.
48. Zak, A.; Sallacanecker, L.; Efrati, R.; Drangai, L.; Fleischer, N.; Tenne, R. Large-scale synthesis of WS_2 multiwall nanotubes and their dispersion. *Sens. Transducers J.* **2009**, *12*, 1–10.
49. Pradhan, G.; Sharma, A.K. Linear and nonlinear optical response of sulfur-deficient nanocrystallite WS_2 thin films. *J. Mater. Sci.* **2019**, *54*, 14809–14824. [CrossRef]
50. Panigrahi, P.K.; Pathak, A. Microwave-assisted synthesis of WS_2 nanowires through tetrathiotungstate precursors. *Sci. Technol. Adv. Mater.* **2008**, *9*. [CrossRef]
51. Zhou, J.; Ma, C.; Kang, X.; Zhang, L.; Liu, X.L. Effect of WS_2 particle size on mechanical properties and tribological behaviors of Cu-WS_2 composites sintered by SPS. *Trans. Nonferrous Met. Soc. China* **2018**, *28*, 1176–1185. [CrossRef]
52. Sharma, S.S.; Bhagat, S.; Singh, J.; Singh, R.C.; Sharma, S.S. Excitation-dependent photoluminescence from WS_2 nanostructures synthesized via top-down approach. *J. Mater. Sci.* **2017**, *52*, 11326–11336. [CrossRef]
53. An, V.; Irtegov, Y.; De Izarra, C. Study of tribological properties of nanolamellar WS_2 and MoS_2 as additives to lubricants. *J. Nanomater.* **2014**, *2014*. [CrossRef]
54. Hazarika, S.J.; Mohanta, D. Inorganic fullerene-type WS_2 nanoparticles: Processing, characterization and its photocatalytic performance on malachite green. *Appl. Phys. A Mater. Sci. Process.* **2017**, *123*, 381. [CrossRef]
55. Huh, S.H. X-ray diffraction of multi-layer graphenes: Instant measurement and determination of the number of layers. *Carbon N. Y.* **2014**, *78*, 617–621. [CrossRef]
56. Khalaj, M.; Zarabi Golkhatmi, S.; Alem, S.A.A.; Baghchesaraee, K.; Hasanzadeh Azar, M.; Angizi, S. Recent Progress in the Study of Thermal Properties and Tribological Behaviors of Hexagonal Boron Nitride-Reinforced Composites. *J. Compos. Sci.* **2020**, *4*, 116. [CrossRef]
57. Malizia, A.; Rossi, R.; Cacciotti, I. Improvement of the shadow tracking setup as a method to measure the velocities values of dark dust in order to reduce the risks of radioactive releases or explosions. *Rev. Sci. Instrum.* **2018**, *89*, 083306. [CrossRef] [PubMed]
58. Klotz, B.R.; Kellogg, F.R.; Klier, E.M.; Dowding, R.J.; Cho, K.C. Characterization, Processing, and Consolidation of Nanoscale Tungsten Powder. 2009. Available online: https://www.researchgate.net/publication/235189436_Characterization_Processing_and_Consolidation_of_Nanoscale_Tungsten_Powder (accessed on 10 December 2020).
59. Yang, C.; Tartaglino, U.; Persson, B.N.J. Influence of surface roughness on superhydrophobicity. *Phys. Rev. Lett.* **2006**, *97*, 116103. [CrossRef] [PubMed]
60. Hazarika, S.J.; Mohanta, D. Revealing mechanical, tribological, and surface-wettability features of nanoscale inorganic fullerene-type tungsten disulfide dispersed in a polymer. *J. Mater. Res.* **2019**, *34*, 3666–3677. [CrossRef]
61. Archard, J.F. Contact and rubbing of flat surfaces. *J. Appl. Phys.* **1953**, *24*, 981–988. [CrossRef]